



**HAL**  
open science

# Image-based river discharge estimation by merging heterogeneous data with information entropy theory

Nour Chahrour, William Castaings, Eric Barthélemy

## ► To cite this version:

Nour Chahrour, William Castaings, Eric Barthélemy. Image-based river discharge estimation by merging heterogeneous data with information entropy theory. *Flow Measurement and Instrumentation*, 2021, 81, pp.102039. 10.1016/j.flowmeasinst.2021.102039 . hal-03750436

**HAL Id: hal-03750436**

**<https://hal.inrae.fr/hal-03750436v1>**

Submitted on 16 Oct 2023

**HAL** is a multi-disciplinary open access archive for the deposit and dissemination of scientific research documents, whether they are published or not. The documents may come from teaching and research institutions in France or abroad, or from public or private research centers.

L'archive ouverte pluridisciplinaire **HAL**, est destinée au dépôt et à la diffusion de documents scientifiques de niveau recherche, publiés ou non, émanant des établissements d'enseignement et de recherche français ou étrangers, des laboratoires publics ou privés.



Distributed under a Creative Commons Attribution - NonCommercial - NoDerivatives 4.0 International License

# Image-based river discharge estimation by merging heterogeneous data with information entropy theory.

CHAHROUR Nour<sup>a,b</sup>, CASTAINGS WILLIAM<sup>b</sup>, BARTHÉLEMY Eric<sup>c,\*</sup>

<sup>a</sup>Univ. Grenoble Alpes, CNRS, INRAE, 38000 Grenoble, France

<sup>b</sup>TENEVIA, 38240 Meylan, France

<sup>c</sup>Univ. Grenoble Alpes, CNRS, Grenoble INP, LEGI, 38000 Grenoble, France

---

## Abstract

An information entropy based approach for the discharge measurements is evaluated for the gaging of the Isère river at the Grenoble university campus. Over a four month period, six discharge measurements were made using a vessel-mounted aDcp. Simultaneously, particle tracking velocimetry (PTV) from video images was used to estimate surface velocities. The surface velocities are projected along the regularly surveyed river section of the Isère-Campus gaging station. The vertical velocity profile at each stream-wise location is approximated by a 1D entropy profile. Information entropy 1D velocity vertical profile depends on two parameters which are fitted using aDcp and surface velocity measurements. The inclusion of the surface velocities reduces the dispersion of the estimated entropy parameters. The measurements show that the two parameters are linearly related with a slope that is stage dependent and thus, surface velocity dependent. From there, the information entropy theory for 1D velocity distribution offers a protocol by which surface velocities only are used to compute the discharges. The protocol is calibrated with both aDcp and surface velocity measurements. It is finally validated with several events during which only surface velocities are measured. For the high water flood event the estimated discharge falls within 2% of the one estimated with the rating curve of the gaging station.

*Keywords:* river, discharge, surface velocity, video, information entropy, gaging curve, aDcp

---

## 1. Introduction

Discharge measurements in natural streams and rivers are of fundamental interest for hydrology and water resources management. Estimating river discharges is therefore paramount for flood mitigation, predicting hydro-electrical production, urban planning, hydraulic structure design, the calibration of hydrological models and many other water related issues.

The discharge or flow  $Q$  is the volume of water crossing the flow area per unit time and no instrument measures it directly. Because it is the flux of the water, traditional approaches to discharge evaluations break down to the estimation of the stream wise water velocity distribution across the river flow area. This distribution is surveyed at specific locations along selected

---

\*Corresponding author

Email addresses: [nour.chahrou@grenoble-inp.fr](mailto:nour.chahrou@grenoble-inp.fr) (CHAHROUR Nour), [william.castaings@tenevia.com](mailto:william.castaings@tenevia.com) (CASTAINGS WILLIAM), [eric.barthelemy@grenoble-inp.fr](mailto:eric.barthelemy@grenoble-inp.fr) (BARTHÉLEMY Eric)

Preprint submitted to *Flow Measurement & Instrumentation*

July 25, 2021

10 verticals. Pairs of adjacent verticals define panels of the cross-section spanning the entire wa-  
11 ter column. An elementary discharge through each panel can be estimated. Methods differ on  
12 how a velocity is assigned to the panel. For measurements using flow meters with propellers  
13 the panels can span the entire water column while with surface aDcp's (acoustic Doppler current  
14 profilers) parts of the panels close to the free surface and the bottom are not surveyed. These  
15 parts are known as blanking zones. The uncertainties of this type of panel method are discussed  
16 by Le Coz et al. (2012).

17 Rating curve techniques measure a flow variable, usually at a low cost, such as the free  
18 surface elevation or the free surface slope (Rantz, 1982; Manfreda et al., 2020). They are said to  
19 be continuous in the sense that these instruments can be set up to measure all the time at given  
20 sampling frequency as long as the data storage capacity allows for it. However, these continuous  
21 methods require calibration. They imply gaging the river discharge now and then to provide a  
22 correspondence between  $Q$  and the flow variable that is measured. This correspondence takes the  
23 form of a so-called rating curve. Discharge gaging techniques such as an aDcp can be sensitive  
24 to the presence of sediment load (suspended or bed load) but also dangerous and impossible to  
25 deploy during floods. For all these reasons, alternative methods have been developed for decades  
26 such as video imaging or radar probing of free surface water velocities.

27 Video image-based methods are extensions of conventional PIV (Particle Image Velocimetry)  
28 which has been used for many decades in experimental fluid dynamics. Using the same principles  
29 based on the analysis of the cross-correlation of image patterns, the extension and adaptation to  
30 large scale flows (LSPIV) was pioneered by Fujita and Komura (1994). This technique became  
31 widely used in river hydrometry for the measurement of surface velocities and the estimation of  
32 discharge (Fujita, 1997; Creutin et al., 2003; Muste et al., 2008; Le Coz et al., 2010). In order  
33 to reduce the impact of the heterogeneity and variability of surface textures, the influence of  
34 lighting conditions and shooting angle, variants such as Particle Tracking Velocimetry (PTV)  
35 and Space-time Image Velocimetry (STIV) were developed or adapted. While PTV is based on  
36 the detection and tracking of individual particles using cross-correlation, optical flow or other  
37 techniques (Tauro et al., 2019; Perks, 2020), STIV stacks image frames along a few search lines  
38 in the flow direction and searches for gradients in the resulting space-time image (Fujita et al.,  
39 2007, 2019). In practice many motion estimation methods used in computer vision can be used.

40 Discharge estimations from surface video based velocities require at least two extra pieces  
41 of information. Firstly, since all these methods provide surface velocities measurements, some  
42 assumptions need to be invoked to transform these surface velocities in vertically averaged ve-  
43 locities. The velocity index  $k_v$  is as straightforward way of linking a surface velocity to a vertical  
44 average velocity. Secondly, the other piece of information required is the bathymetry/water depth  
45 cross wise distribution necessary to compute a volume flux through the water column.

46 The idea of the velocity index goes back to (De Prony, 1804; Dulos, 1877, p. 73) and  
47 continues to be a subject of applied research (Gunawan et al., 2012; Moramarco et al., 2017;  
48 Kästner et al., 2018). The flow shallowness of large rivers (top width much larger than the depth)  
49 is expected to shape velocity distributions to be two-dimensional, and the velocity vertical pro-  
50 file is deemed to follow amongst others the classical logarithmic law or Prandtl's seventh power  
51 law over the water depth (Cheng, 2007). In the latter case, the theoretical velocity index for  
52 the seventh power law is  $k_v = 0.875$ . The value of the velocity index depends on the shape of  
53 the vertical velocity profile which is a signature of the boundary layer vertical structure. This  
54 velocity index also depends on how close from the banks the vertical is. Indeed, the velocity dis-  
55 tribution is strongly influenced by bank induced friction (Mueller, 2013) and secondary currents.  
56 The boundary layer is affected by the turbulence of the flow which depends on the flow aspect

57 ratio, on the bed-roughness, on bed forms, the Froude and the Reynolds numbers.

58 Assumptions on the velocity vertical profile are also used in aDcp commercial softwares to  
59 complement the vertical profile in the blanking zones near the free surface and the bottom. The  
60 log-profile and 1/6th or 1/7th power laws are the most popular way of extrapolating for velocity  
61 values outside the measured range of water column (Le Coz et al., 2012). Strictly speaking the  
62 log-profile is not supposed to describe the velocity distribution of the top 70 to 80% of the  
63 water column (Nezu and Nakagawa, 1993). Power law profiles are mere approximations with  
64 little physical grounds. The information entropy (Shannon, 1948; Jaynes, 1957) provides an  
65 interesting alternative.

66 The maximization of the entropy (Jaynes, 1957) ensures that the probability distribution as-  
67 signed to a series of values of a random variable subject to physical constraints, is the least biased  
68 (Jaynes, 2003). By information entropy theory, velocity profiles are derived by maximizing the  
69 entropy that depends on three parameters, the surface velocity  $u_s$  and two Lagrange multipliers  
70 in the case of two integral constraints (Chiu, 1987; Singh, 2014). The surface boundary condi-  
71 tion imposes a relationship between these three parameters. Chiu (1987) showed that 1D vertical  
72 profiles derived from the information entropy theory match very closely the measured profiles, a  
73 result verified and refined by many later studies (Luo et al., 2018; Yeganeh and Heidari, 2020).  
74 As explained by Chiu (1987) fitted entropy-based profiles can be connected to log profile char-  
75 acteristics and especially used to determine the friction velocity. The study by Chiu (1987) has  
76 triggered a large amount of investigation using information entropy.

77 Information entropy theory can also be applied to describe 2D velocity distributions in a  
78 cross-section of a river Chiu (1988); Singh (2014). Because of the geometric extra degree of  
79 freedom compared to 1D cases, entropy based 2D distributions theories resort to assumptions on  
80 the shape of the isovel pattern in the cross-section (Chiu, 1988; Moramarco et al., 2004, 2017,  
81 2019). These assumed isovel distributions have been thoroughly validated (Marini et al., 2017).  
82 This opens the way to discharge evaluations without any prior bathymetry surveys. Very recently  
83 such approach was effectively rendered operational by Moramarco et al. (2019) using develop-  
84 ments of Moramarco et al. (2004) in such a way that allows discharge evaluations using satellite  
85 data such surface water velocity and elevation.

86 Entropy maximization yields a widely used relation between  $u_{max}$  and the cross-sectional  
87 average velocity  $U$  (Chiu, 1988, 1991; Chiu and Said, 1995),

$$88 \quad U = u_{max} \Phi(M) \quad (1)$$

89 where  $\Phi$  is a uniquely defined function and  $M$  the so-called entropy parameter. Empirical ob-  
90 servations (Chiu and Said, 1995; Chen and Chiu, 2004; Moramarco et al., 2004; Chiu and Hsu,  
91 2006; Fulton and Ostrowski, 2008; Ardiclioglu et al., 2012; Moramarco and Singh, 2010; Moramarco et al.,  
92 2017) show that  $M$  only depends on the river cross-section and thus that equation (1) is a one-  
93 to-one relation. In 2D distributions the maximum velocity does not necessarily occur at the free  
94 surface, a characteristic known as the dip phenomenon (Moramarco et al., 2017). This implies  
95 that discharge estimations based on (1) require exploring the velocity distribution within the flow  
96 area to determine  $u_{max}$ , an exploration only accessible to sophisticated methods such as aDcp's.  
97 Moreover, (1) implicitly allows for only one local maximum  $u_{max}$  in the cross-section which is  
98 not necessarily the case in river sections downstream of bends and meanders or with secondary  
99 currents. More generally it is reasonable to presume that because of the 3D nature of the flow  
100 with the complex distribution of secondary currents and the river geometry, the isovel patterns  
101 parametrization as given by Chiu (1988); Kumbhakar et al. (2019) is too schematic even though,

102 as indicated previously, it is relevant for ungaged rivers (Moramarco et al., 2019). Therefore, in  
 103 the present study we re-analyze 1D entropy-based distributions for video-based discharge esti-  
 104 mations in regularly gaged rivers.

105 In section 2, the standard 1D information entropy theory is recalled. We show that it yields a  
 106 relationship between surface velocity measurements and velocity vertical profiles characteristics  
 107 allowing for easy discharge evaluations. Section 3 describes the gaging station where aDcp, sur-  
 108 face imaging and stage data are acquired and at which a longstanding rating curve is available  
 109 for our method validation. Section 4 discusses how reliable the sole use of video-based surface  
 110 velocities is for discharge estimations. We conclude in Section 5.

## 111 2. Information entropy theory & discharge evaluations

112 For 1D vertical profiles, the time average stream-wise velocity  $u$  is assumed to be a random  
 113 variable with a probability density function denoted  $p(u)$ . The Principle of Maximum Entropy  
 114 (POME) is used to find the best fit distribution of velocity by maximizing the entropy of  $p(u)$   
 115 subject to the basic constraints. Information entropy (Shannon, 1948; Jaynes, 1957; Chiu, 1987,  
 116 1988) which is a measure of the average information content in a set of observed velocity values  
 117  $u$ , is expressed as

$$118 \quad H = - \int p(u) \ln(p(u)) du \quad (2)$$

119 where  $p(u)$  is the probability density function of the velocity values and the integral taken over all  
 120 possible values of  $u$ . Definition (2) is referred to as the Shannon entropy. Other definitions such  
 121 as the Tsallis or Renyi entropies are also used to define and approximate velocity distributions  
 122 (Yeganeh and Heidari, 2020). The function  $p(u)$  is by definition related to  $F(u)$ , the cumulative  
 123 distribution function (CDF), in the following way,

$$124 \quad F(u) = \text{probability that (velocity} \leq u) \quad (3)$$

$$125 \quad p(u) = \frac{dF}{du} \quad (4)$$

126 The probability density function  $p(u)$  is subject to the following constraints (Chiu, 1987, 1988),

$$127 \quad \int_0^{u_{max}} p(u) du = 1 \quad (5)$$

$$128 \quad \int_0^{u_{max}} u p(u) du = \bar{u} \quad (6)$$

129 where  $u_{max}$  is the maximum velocity value,  $\bar{u}$  the expected velocity. In the case of 1D profiles in  
 130 wide channels Marini and Fontana (2020) showed that  $\bar{u}$  is same as  $U$ , the vertical average. The  
 131 Principle of Maximum Entropy (POME) (Chiu, 1987, 1988) involves not only (2) but also two  
 132 Lagrange multipliers  $\lambda_1$  and  $\lambda_2$  associated to (5) and (6). Details of the calculus of variations are  
 133 in Chiu (1987, 1988). It yields,

$$134 \quad p(u) = e^{\lambda_0} e^{\lambda_2 u} \quad (7)$$

$$135 \quad \lambda_0 = \lambda_1 - 1 \quad (8)$$

136 Obtaining the velocity distribution  $u$  requires some assumption on  $p(u)$ . In this paper, we  
 137 focus on 1D distributions or said differently to rivers/channels wide compared to the water depth

138 (Chiu and Hsu, 2006). To that end Chiu (1987) assumed a monotonously increasing vertical  
 139 velocity profile from bottom to the free surface. Thus  $F(u)$  is the fraction of water column with  
 140 all velocities smaller than  $u$ . This writes,

$$141 \quad F(u(z)) = \frac{z}{D} \quad (9)$$

142 where  $D$  is the total water depth and  $z = 0$  is the bottom. This form of CDF also implies that the  
 143 maximum velocity  $u_{max}$  lies at the surface. The probability density function now writes,

$$144 \quad p(u) = \frac{1}{D} \frac{dz}{du} \quad (10)$$

145 Equating (7) to (10), integrating once and applying the boundary condition,

$$146 \quad u = 0 \quad \text{at} \quad z = 0 \quad (11)$$

147 gives the mean stream-wise velocity profile expression,

$$148 \quad u = \frac{1}{\lambda_2} \ln \left[ 1 + \lambda_2 e^{\lambda_0} \frac{z}{D} \right] \quad (12)$$

149 where  $\lambda_2$  is dimensionally the inverse of a velocity and is found to be positive in the experiments.  
 150 Many authors (Chiu, 1987, 1988) fit measured vertical profiles of streamwise velocity with (12)  
 151 by calibrating the two free parameters  $\lambda_2$  and  $\lambda_0$ . An alternate expression of  $u$  stems from the  
 152 boundary condition,

$$153 \quad u = u_s \quad \text{at} \quad z = D \quad (13)$$

154 or equivalently from (5) that gives a relationship between  $\lambda_2$  and  $\lambda_0$  that involves the surface  
 155 velocity  $u_s$  of the profile,

$$156 \quad \lambda_0 = \ln \lambda_2 - \ln \left( e^{\lambda_2 u_s} - 1 \right) \quad (14)$$

157 and the following mean velocity profile expression,

$$158 \quad u = \frac{1}{\lambda_2} \ln \left[ 1 + \left( e^{\lambda_2 u_s} - 1 \right) \frac{z}{D} \right] \quad (15)$$

159 The key idea of the present study is to only use surface velocity measurements combined with  
 160 the cross-section bathymetry to evaluate the discharge of large streams. In a wide channel (top  
 161 width larger than depth), lateral bank friction has little influence on the isovel pattern. Isovels are  
 162 nearly horizontal with therefore monotonously increasing velocities from bottom to free surface.  
 163 Thus, each vertical profile can be advantageously fitted by a 1D velocity profile such as (12).  
 164 The sole knowledge of  $u_s$  is not sufficient to compute the discharge with (15), the value of the  
 165 Lagrange multiplier  $\lambda_2$  is necessary. The extra assumption we introduce stems from an empirical  
 166 observation by Singh (2014) in the case of 2D distributions that indicates a linear relationship  
 167 between the two Lagrange multipliers. We assume that it is also true in 1D distributions and  
 168 this will be verified in the course of this work. Therefore, we hypothesize that for a given water  
 169 level or equivalently a given discharge,  $\lambda_0$  and  $\lambda_2$  for all verticals are linearly related. The rate of  
 170 change of  $\lambda_0$  with  $\lambda_2$  derived from (14) writes,

$$171 \quad m = \frac{\partial \lambda_0}{\partial \lambda_2} = \frac{1}{\lambda_2} - \frac{u_s e^{\lambda_2 u_s}}{e^{\lambda_2 u_s} - 1} \quad (16)$$

172 In situations where  $\lambda_2 u_s$  is large, such as in the case of wide streams, this relation rewrites as,

$$173 \quad \lambda_2 = \frac{1}{m + u_s} \quad (17)$$

174 This last relation will enter the following protocol. Vertical profiles of the horizontal velocity  
175 measured by aDcp, complemented with video surface velocities measurements, are approximated  
176 with (12) by calibrating  $\lambda_2$  and  $\lambda_0$ . This provides a set of quasi-straight lines (Singh, 2014),  
177 parametrized by  $u_s$  the surface velocity. These lines will be linearly fitted to yield a calibrated  
178  $m$ , which is nothing else than rating the  $m$  values with  $u_s$ . Once this rating is robust enough,  
179 any surface velocity measurement  $u_s$  can be associated to a  $m$  value. By (17)  $u_s$  and  $m$  are then  
180 used to compute  $\lambda_2$  which in turn allows the evaluation of the unitary discharge  $q$  at the given  $X$   
181 cross-wise location. An analytical expression of the unitary discharge  $q$  is easily computed from  
182 (15) by simple integration,

$$183 \quad q(X) = \int_0^{D(X)} u \, dz = \frac{D(X)}{\lambda_2} \frac{1}{e^{\lambda_2 u_s} - 1} \left[ 1 + (e^{\lambda_2 u_s} - 1)(\lambda_2 u_s - 1) \right] \quad (18)$$

184 Using formula (18) to compute  $q$  requires the knowledge of  $D(X)$  the water depth at the different  
185 cross wise locations. Once the set of cross wise  $q(X)$  values is computed, a numerical integration  
186 from the left bank  $X$  to the right bank  $X$  yields the total discharge  $Q$ .

### 187 3. Case study and available measurements

188 The Isère-Campus gaging station is located on the banks of the Isère River, a few kilome-  
189 ters upstream of Grenoble (France) on the main campus of the University of Grenoble-Alpes.  
190 Figure 1 shows an upstream bend and a bridge (130 m upstream of the gaging station). The  
191 bridge has no pier in the river thus generating no perturbations at the gaging station. The river  
192 bottom slope is  $S_0 = 0.5 \cdot 10^{-3}$ . The inter-annual average discharge of the Isère at Grenoble is  
193  $179.0 \text{ m}^3/\text{s}$ . The station is equipped for measuring and exploring river discharge, water level,  
194 water temperature, turbidity, concentration of suspended solids, and the velocity fields.

195 An unmanned vessel-mounted acoustic Doppler current profiler (aDcp; Nortek Rio Grande,  
196 1200 kHz operated with WIN-RIVER II) collected velocity profiles of the entire channel to cal-  
197 culate channel velocities and discharge. The vessel is attached to a cable-way system spanning  
198 over the transect of the Isère river at the station. The cable-way system tows the vessel at the free  
199 surface across the transect. The aDcp sensors are located 0.1 m below the water surface. The  
200 aDcp has a blanking distance of 0.5 m, resulting in a measurement range from approximately  
201 0.6 m below the water surface down to the top of the blanking zone near the river bottom. The  
202 blanking zone at the bottom is 0.6 m. Velocity data were collected at vertical cells of 0.10 m to  
203 0.20 m in size at a frequency of roughly 1 Hz. In the present study two methods were used for  
204 the velocity profiles and discharge. One called continuous crossing method implied towing the  
205 aDcp across the river at nearly constant speed of roughly 0.18 m/s and the other called fixed ver-  
206 tical method for which the aDcp was stationary at a discrete and finite number of locations in the  
207 transect. The bottom-tracking mode of the aDcp was enabled both for the continuous crossings  
208 and fixed verticals. For the fixed vertical method, roughly 100 vertical profiles were recorded  
209 at each cross-wise position. In this case the discharge is computed with the midsection method.  
210 The panel assigned to a vertical is in that case centered on the vertical with left and right limits  
211 are midway from the adjacent verticals.



Figure 1: Top view and location (red point) of the Isère-Campus gaging station. Aerial image obtained from Imagery @2018 Google. The width of the river is roughly 60 m at the gaging station.

212 The station is also equipped with a staff gage installed on the left bank side to measure the  
 213 stage (water level)  $H$  with a resolution of 1 cm. This stage measure is used in conjunction with a  
 214 discharge rating curve  $Q_{RC}$ . The rating curve is a best fit power law based on discharge and stage  
 215 measurements done at the Isère-Campus station between 1992 and 2018.

216 Table 1 provides an overview of all the experiments used in this work, including the deployed  
 217 instruments. The bottom-tracking of the aDcp was used to determine the average cross-section  
 218 bathymetry which is necessary for the discharge computation by the entropy method (see eq.18).  
 219 Different types of measurements were combined to this end. The bathymetric surveys of the 5  
 220 continuous crossings for  $H = 0.8$  m are averaged. This low discharge case does not allow for the  
 221 higher parts of the bathymetry to be measured. To overcome this, the  $H = 2.04$  m fixed vertical  
 222 survey is used. The resulting average bathymetry is given in Figure 2. The cross-section shape is  
 223 close to triangular. The right bank has a mild slope due to an alternate gravel bank whereas the  
 224 right bank is steeper.

225 A video surveillance camera AXIS P1357-E (5 megapixels, 12 frames per second) was in-  
 226 stalled on the left bank. In order to reduce the transmission bandwidth and enable the real-time  
 227 processing on a remote server (cloud computing), a burst of 4 images separated by 80 ms (median  
 228 value) is sent by the camera to an FTP server. The camera was calibrated by the topographical  
 229 survey of ground reference points visible in the camera image.

230 Over a region of 20 meters around the surveyed profile, the surface velocity vector field is



date	$H$ (m)	aDcp method		surface velocity measurements	rating curve discharge $Q_{RC}$ ( $m^3/s$ )
		number of fixed verticals	number of continuous crossings		
18/10/2017	0.8	9	5	no	61.16
07/12/2015	1.275	none	4	no	105.72
01/12/2016	1.83	16	6	no	171.34
19/03/2018	2.04	20	none	yes	198.37
04/05/2018	2.92	none	6	yes	320.72
24/04/2018	3.02	none	8	yes	335.35
11/06/2018	3.39	27	none	yes	390.3
23/01/2018	4.05	none	6	yes	491.57
05/01/2018	5.18	none	none	yes	674.9

Table 1: Conditions and parameters of the different surveys. The stage reading is  $H$ .

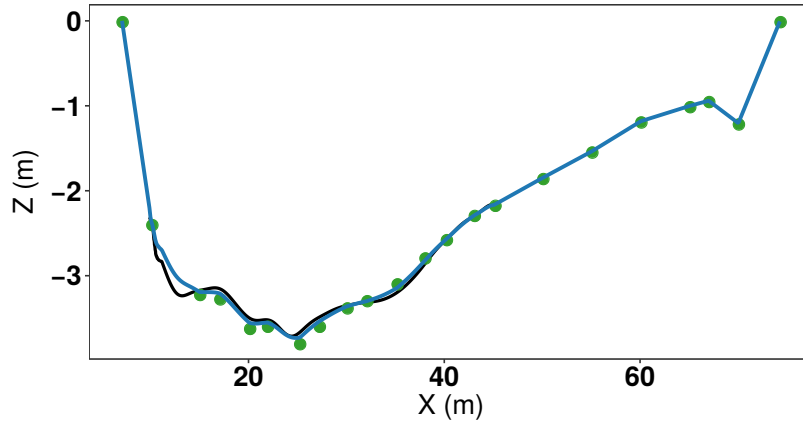


Figure 2: Cross section bottom profile at the Isère-Campus gaging station. Green dots: fixed vertical measurements for  $H = 2.04$  m; black line: average bottom bathymetry of the 5 continuous crossings for  $H = 0.8$  m; blue curve: average of these two bathymetries. The  $X$  axis is along the transect.  $Z = 0$  corresponds to the free surface level for the stage  $H = 2.04$  m.

231 measured by a PTV algorithm between successive images. The spatial resolution of this mea-  
232 sured field is below 1 m. A consolidated vector field is then obtained for each burst of 4 images  
233 (Figure 3-a). A smoothing approach is used for the estimation of the streamwise surface velocity  
234 profile. The surface velocity field of Figure 3-a is projected and interpolated on the cross wise  
235 transect (see Figure 4 and Figure 3-b). The profile is extrapolated to the banks using the con-  
236 servation of the Froude number hypothesis (Fulford and Sauer, 1986). This is useful for surface  
237 velocities far from the camera and especially close to the right bank. The median value of the  
238 proportion of extrapolated surface velocity profile is approximately 5%. The velocity accuracy  
239 depends on the location on the profile (i.e. more dispersion on the right river bank), on the wa-



a)



b)

Figure 3: Surface fluid velocities extracted from surface video images on the 23/01/2018 for a stage of  $H = 4.03$  m. a): raw PTV surface velocity vectors; b): estimated streamwise velocity profile. Color-bars are on the left of the images. River flowing from right to left and camera on the left bank.

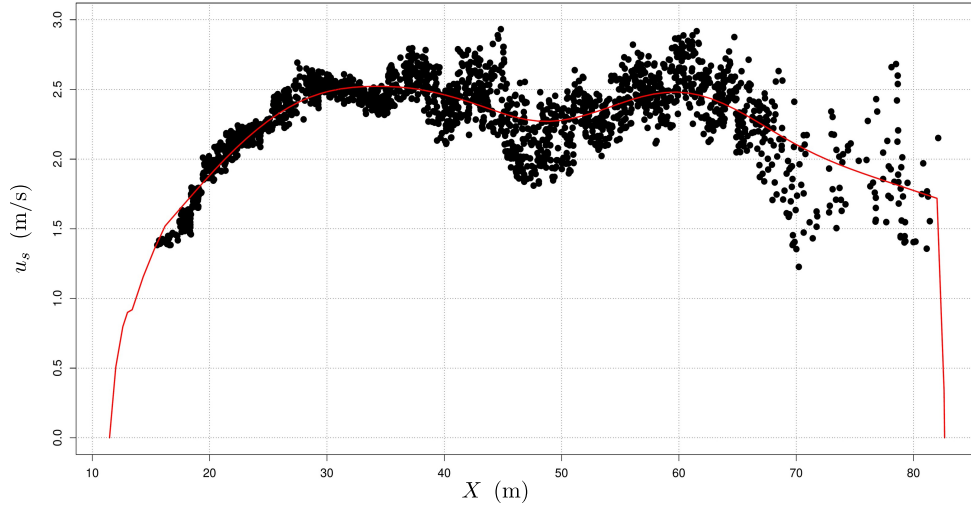


Figure 4: Surface velocity field  $u_s$  projected and interpolated on the surveyed cross section same date as in Figure 3 (23/01/2018) for a stage of  $H = 4.03$  m.  $X$ : cross-wise coordinate. Black dots: velocity values. Red curve: best fit and same curve as in Figure 3-b.

240 ter level and on the illumination conditions. Overall, the relative error on the average surface  
 241 velocity is between 2 % and 15 %.

#### 242 4. Application

243 Fitting a time average velocity vertical profile is the initial step in the rating procedure of  $m$   
 244 by  $u_s$ . The time averaging for the fixed vertical method is obvious since for each verticals, cor-  
 245 responding to a cross wise position  $X$ , the vessel is stationary for a few minutes while it samples  
 246 a sufficient number of instantaneous velocity vertical distributions. In contrast, for the contin-  
 247 uous crossing method the vessel is towed along the transect of the cross-section measuring more  
 248 than 200 verticals with unreferenced positions with respect to  $X$ . In this case, it was decided to  
 249 average bins of 15 adjacent verticals together and then interpolate the obtained averaged velocity  
 250 vertical distributions on a given  $X$  grid. This bin averaging is deemed to be equivalent to a time  
 251 averaging since the vessel speed towed by the cable-way is small (of order 0.18 m/s) compared  
 252 to the sampling rate of the aDcp (1 Hz).

253 Examples of time averaged horizontal velocity distribution profiles are plotted in Figure 5.  
 254 They correspond to different verticals at different distances to the left bank of the cross-section.  
 255 The fitted entropy-based velocity distributions are computed by merging the aDcp measurements,  
 256 the surface video-based velocities and a bottom velocity imposed at zero value. The highest  
 257 number of measured values on each vertical are those of the aDcp, they therefore strongly con-  
 258 strain the approximation. Video-based surface velocities are slightly scattered with respect to the  
 259 entropy-based velocity distribution. However, the addition of video surface velocity data for the  
 260 fitting improves the entropy parameter estimations. Figure 6 shows that the scatter of  $\lambda_1$  and  $\lambda_2$   
 261 is significantly reduced by the incorporation of a surface velocity in the data used for the fitting.  
 262 The relationship between  $\lambda_1$  and  $\lambda_2$  clearly benefits from this addition.

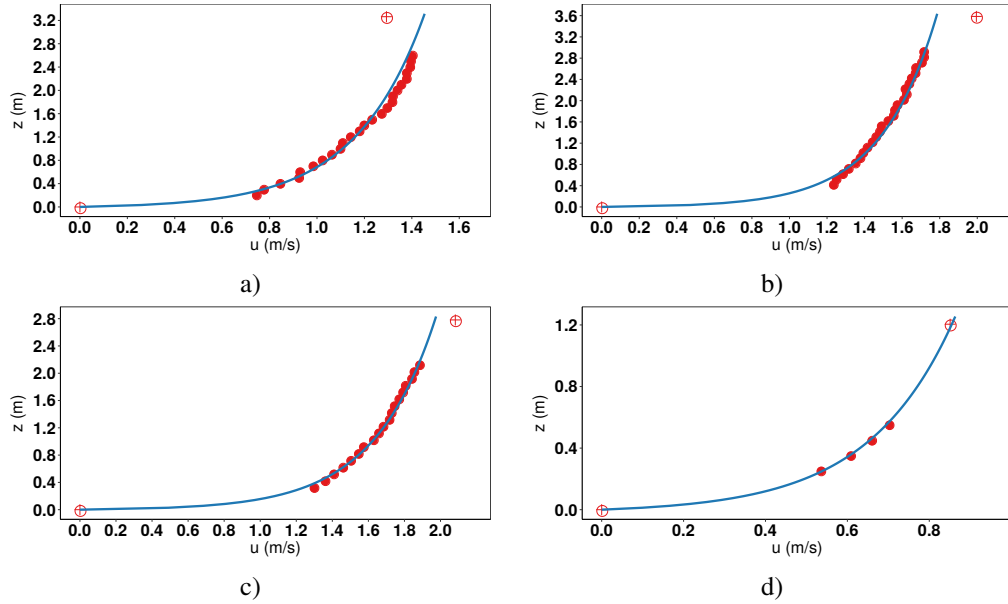


Figure 5: Calibration of entropy-based vertical velocity distributions. Stage  $H = 2.04$  m case. a):  $X = 17.07$  m; b):  $X = 27.23$  m; c):  $X = 38.02$  m; d):  $X = 70.04$  m. Red dots: aDcp measurements. Top circle/cross point: video surface velocity. Bottom points at  $z = 0$ : circle/cross. Blue line: entropy-based velocity fitting. The  $z$  axis is the local vertical axis.

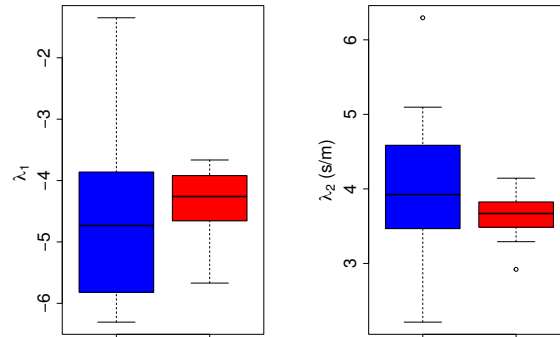


Figure 6:  $\lambda_1$  and  $\lambda_2$  boxplot distributions. blue boxplots:  $\lambda_1$  and  $\lambda_2$  determined with no video surface velocity incorporated in the fitting of (15); red boxplots: determined with video surface velocity incorporated in the fitting of (15). Stage at  $H = 2.04$  m. Box: 2nd and 3rd quartile group; black line in the box: median value; whiskers: 1st and 4th quartile; dots: outliers

263 This entropy-based velocity distribution provides an extrapolation near the bed and below the  
 264 surface in the blanking zones. It is interesting since the unitary discharge  $q(X)$  is most sensitive to  
 265 the near surface extrapolation because it corresponds to water layers with the highest velocities.  
 266 A first check, summarized in Table 2, is undertaken to assess if entropy-fitted vertical profiles  
 267 yield correct discharge estimates. On the one hand (“adcp” column of Table 2)  $q(X)$  is estimated  
 268 by a numerical integration by the trapezoidal rule of the vertical profile as given by the aDcp

269 measurements with or without surface velocity estimations. On the other hand (“entropy” column  
 270 of Table 2)  $q(X)$  is computed by (18) for which  $\lambda_2$  and  $u_s$  are provided for each vertical by the  
 271 entropy fitting procedure. For both approaches the total discharge  $Q$  is given by the numerical  
 272 integration bank to bank of the cross-wise  $q(X)$  curve. Such procedure has been applied to 5 cases  
 273 of Table 1 and the results are given in Table 2. The 5 cases were chosen so that the discharge  
 274 increment between each estimations was roughly  $100 \text{ m}^3/\text{s}$  in order to cover regularly the range  
 275 of discharges. The outcome is that the differences in discharge between the two approaches are  
 small thus validating the use of entropy-based discharge estimate.

$H$ (m)	Discharge ( $\text{m}^3/\text{s}$ )		diff. (%)
	aDcp	entropy	
1.275	122.12	129.15	5.7
2.04	199.43	202.45	1.5
2.92	309.06	320.59	3.7
3.39	400.20	410.82	2.6
4.05	529.27	540.63	2.1

Table 2: Discharge computations. The stage is  $H$ . “aDcp” column: discharge computed by numerical integration of the data points with the adcp data and the video surface velocities when available (not measured for  $H = 1.275 \text{ m}$ ). “entropy” column: discharge computed with the cross-wise integration of (18). “Diff.” column: difference in % between the two approaches.

276  
 277 The ultimate step is to understand and analyze if the discharge can be estimated just with  
 278 video surface velocities. As discussed in section 2 we only have one theoretical relation (16)  
 279 between  $\lambda_1$  (or  $\lambda_0$ ),  $\lambda_2$  and  $u_s$ . So the sole use of surface velocities is conceivable if an extra  
 280 relation between two of the three parameters of (16) is found. It happens that for a given stage,  
 281 thus for a given maximum surface velocity, the pairs  $\lambda_1$  and  $\lambda_2$  at each vertical form a quasi-  
 282 straight line as plotted in Figure 7. This was observed theoretically by Singh (2014) for 2D  
 283 velocity distributions, and it is remarkable that the slope  $m$  of this relation is only a function  
 284 of the surface maximum velocity  $U_{max}$ . This provides the empirical rating between  $m$  and the  
 285 maximum surface velocity  $U_{max}$  we are looking for. Obviously, the more aDcp and surface  
 286 velocity measurements are compiled, the more robust this relationship will be. Figure 8 shows  
 287 that the relation between  $m$  and  $U_{max}$  is linear and thus, can be easily used to extrapolate for  
 288 values outside the range of those already measured and especially at high discharges. Indeed in  
 289 Figure 8 the lowest value corresponds to a discharge  $Q = 61.16 \text{ m}^3/\text{s}$  which is a very low value  
 290 for the Isère since the inter-annual three days average minimum is roughly  $80 \text{ m}^3/\text{s}$ . The slope  
 291  $m$  is negative thus for  $\lambda_2$  to be positive, relation (17) says that  $u_s > |m|$  which is the case as  
 292 evidenced by Figure 8. The best fit line in Figure 8 is given by,

$$|m| = 0.774 U_{max} - 0.0544 \quad \text{with } R^2 = 0.98 \quad (19)$$

294 The assumption of (17) is that  $\lambda_2 u_s$  is large. In Figure 9 the  $\lambda_2 u_s$  cross-wise distribution  
 295 indicates that this quantity is in most positions above 5, a large enough value to make (17) valid.  
 296 Indeed the function  $e^\alpha / (e^\alpha - 1)$  in (16) is within 5 % of 1 for  $\alpha$  above 3.

297 Finally the scheme to compute the discharge for a given stage  $H$  is the following:

- 298 1. video images are processed to supply a surface velocity profile  $u_s(X)$ ;
- 299 2. the surface maximum  $U_{max}$  is extracted;
- 300 3. a unique  $m$  is determined by the “rating” curve of Figure 8 or equivalently with (19);

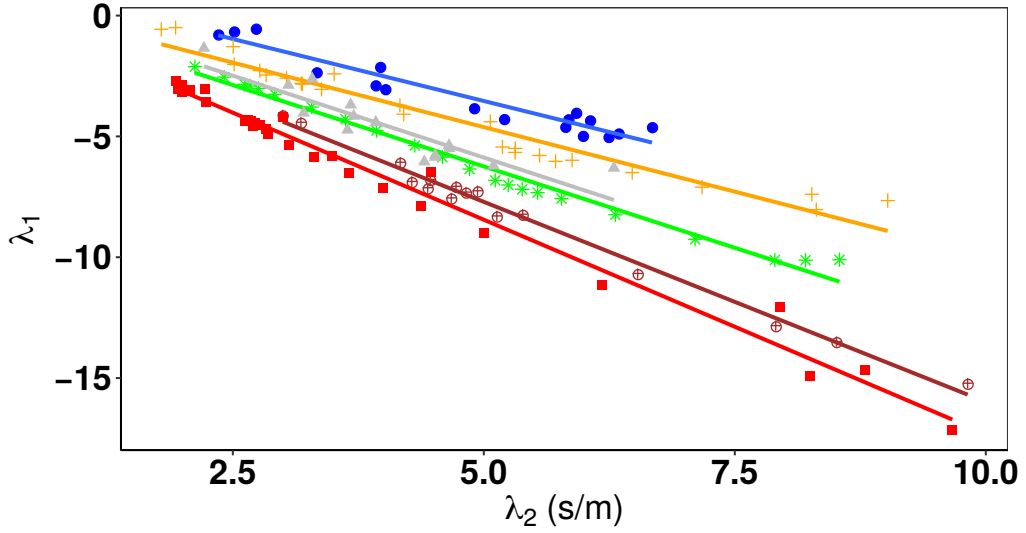


Figure 7: Experimental relationship of  $\lambda_2$  with  $\lambda_1$  for different stages. Color lines: best linear fit of the data (points) of same color. Blue:  $H = 0.8$  m and  $U_{max} = 1.31$  m/s; yellow:  $H = 1.275$  m and  $U_{max} = 1.53$  m/s; green:  $H = 1.83$  m and  $U_{max} = 1.79$  m/s; grey:  $H = 2.04$  m and  $U_{max} = 1.93$  m/s; brown:  $H = 2.92$  m and  $U_{max} = 2.17$  m/s; red:  $H = 4.05$  m and  $U_{max} = 2.42$  m/s.

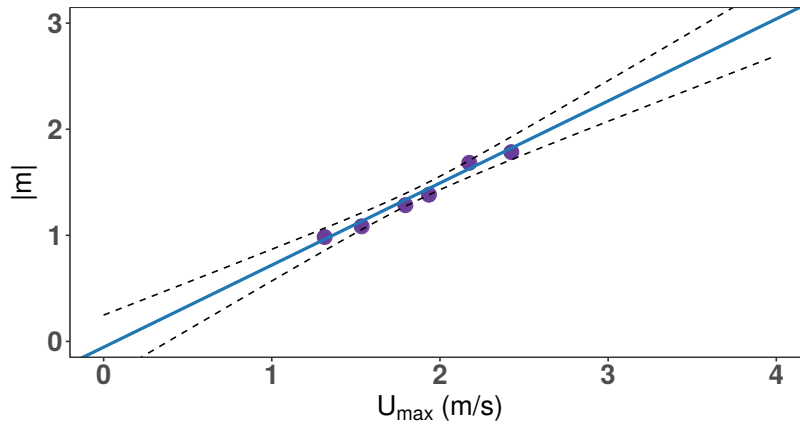


Figure 8: Relation between the module  $|m|$  of the slope (16) and the surface maximum velocity  $U_{max}$ . Purple circles: data; blue plain line: best linear fit regression line; black dashed line: 95 % confidence interval.

- 301 4. relation (17) is used to determine  $\lambda_2(X)$  at each  $X$  where a surface velocity is given;  
 302 5.  $q(X)$  is computed by (18);  
 303 6. a bank to bank numerical integration of  $q(X)$  supplies the total discharge  $Q(H)$ .

304 The scheme described above to determine  $Q$  using only video recorded surface velocities is  
 305 now applied to three cases given in Table 3. For two of the cases  $m$  is not in the range of those of  
 306 Figure 8. The one for  $H = 5.18$  is for a flood situation. For each video surface velocity  $u_s$  along

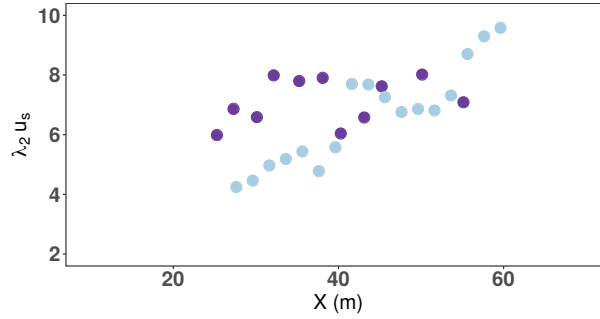


Figure 9: The  $\lambda_2 u_s$  cross-wise distribution. Purple: stage at  $H = 2.04$  m; light blue: stage at  $H = 4.05$  m.

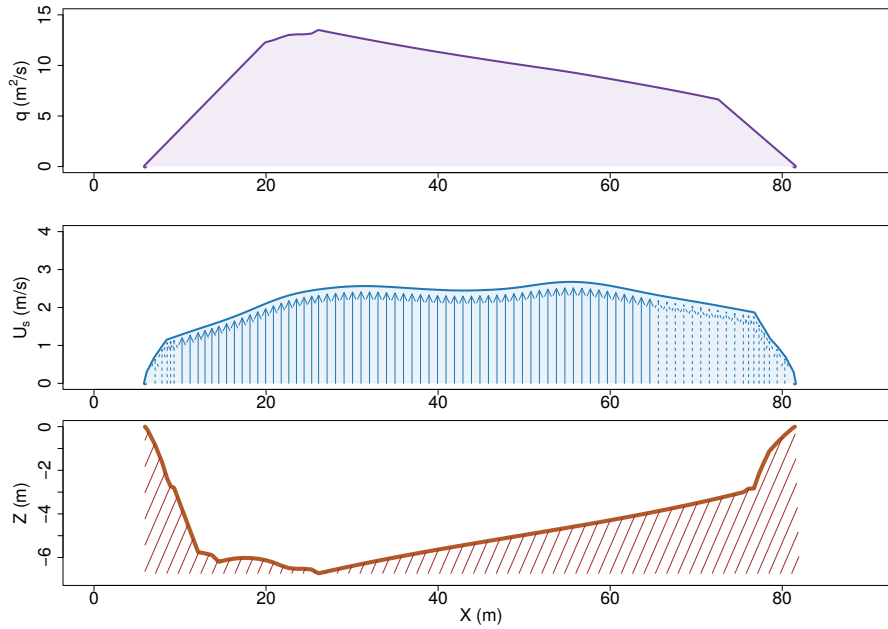


Figure 10: Case with stage at  $H = 5.18$  m with no aDcp measurements. middle panel: interpolated measured video-based surface velocity  $u_s$  distribution; dashed vectors: extrapolated vectors. Top panel: cross-wise distribution of unitary discharge  $q(X)$  by the full entropy method. Bottom panel: cross-section profile,  $Z = 0$  corresponds to the free surface level.

307 the cross-wise transect  $\lambda_2$  is computed by (17) using the unique  $m$  from (19). The  $q$  values along  
 308 the transect are determined by (18). A example of the  $q$  crosswise profile is plotted in Figure 10  
 309 for the  $H = 5.18$  case. In the  $Q$  column of Table 3 the upper bound and lower bound of  $Q$  as  
 310 computed by the 95 % confidence interval on  $m$  of Figure 8 are given. Predicted values are all  
 311 close to the rating curve value  $Q_{RC}$  of the discharge. The uncertainty interval contains the  $Q_{RC}$   
 312 value except for the  $H = 1.66$  case which falls very close at  $4 \text{ m}^3/\text{s}$  from that interval. Recall that  
 313 at this stage of our work, the confidence interval for the “rating” curve Figure 8 is based on only  
 314 6 points. The uncertainties will decrease by incorporating more measurements with time.

date	$H$ (m)	$U_{max}$ (m/s)	$m$	$Q$ (m <sup>3</sup> /s)	$Q_{RC}$ (m <sup>3</sup> /s)	error (%)
13/12/2017	1.66	1.58	-1.17	$170.9 \pm 17.3$	151	13.2
24/04/2018	3.02	2.26	-1.69	$348.8 \pm 20.3$	352	0.9
05/01/2018	5.18	2.64	-1.99	$657.3 \pm 44$	674.9	2.6

Table 3: Video alone discharge evaluations. The stage is  $H$ ;  $U_{max}$  is the maximum video measured surface velocity;  $Q$  the computed total discharge;  $Q_{RC}$  the rating curve discharge associated with  $H$ ; error column is the relative difference between  $Q$  and  $Q_{RC}$ .

315 Noteworthy is the double maximum of the surface velocity in Figure 10 also appearing in  
316 Figure 4 for another stage. This may be due to the river bend roughly 300 meters upstream  
317 (Figure 1). Had we used the 2D entropy based velocity distribution the determination of the  
318 “y-axis” would have been uncertain.

## 319 5. Conclusions

320 In the present study, we have developed, calibrated and validated a novel approach for dis-  
321 charge estimations with image-based surface velocities. The method draws on information en-  
322 tropy derived 1D velocity distributions, applicable to rivers large compared to the water depth.  
323 The method once calibrated only requires surface stream-wise velocities such as those provided  
324 by video imaging. The calibration relies on the rating of the slope  $m$  of the relation between  
325 the two Lagrange multipliers  $\lambda_2$  and  $\lambda_1$  of the information entropy theory. The rating of  $m$  with  
326 the maximum surface stream-wise velocity is provided by conventional aDcp surveys of the  
327 cross-sectional velocity distribution and video-based surface velocities. These heterogeneous  
328 data sources describing different velocity vertical profiles are merged and approximated with  
329 theoretical 1D velocity distributions given by the information entropy theory. Our data confirms  
330 that  $\lambda_2$  and  $\lambda_1$  are indeed linearly related and that the calibration clearly benefits from the addition  
331 of measured surface velocities. The method applied to the Isère river at the Isère-Campus gag-  
332 ing station is totally consistent with the longstanding rating curve between stage and discharge  
333 of this gaging station. The deployment of aDcps with smaller blanking zones could improve  
334 the calibration by providing more information especially in the top layers of the water column.  
335 Furthermore, extra calibration data will be valuable to improve the  $m-U_{max}$  rating curve.

## 336 6. Acknowledgements

337 The first author is very grateful to TENEVIA for the internship grant they offered. We ex-  
338 press our deepest gratitude to Christophe Rousseau for his continuous technical support. We are  
339 thankful to ENSE3 (Ecole Nationale Supérieure de l’Energie, l’Eau, et l’Environnement) and  
340 EDF-DTG (Electricité de France - Direction Technique Générale) for granting us access to the  
341 Isère-Campus gaging station.

## 342 References

- 343 Ardicioglu, M., Genc, O., Kalin, L., Agiralioglu, N., 2012. Investigation of flow properties in natural streams using the  
344 entropy concept. *Water and Environment Journal* 26, 147–154.  
345 Chen, Y.C., Chiu, C.L., 2004. A fast method of flood discharge estimation. *Hydrological Processes* 18, 1671–1684.



- 346 Cheng, N.S., 2007. Power-law index for velocity profiles in open channel flows. *Advances in Water Resources* 30, 1775  
347 – 1784. doi:<https://doi.org/10.1016/j.advwatres.2007.02.001>.
- 348 Chiu, C.L., 1987. Entropy and probability concepts in hydraulics. *Journal of Hydraulic Engineering* 113, 583–600.
- 349 Chiu, C.L., 1988. Entropy and 2-d velocity in open channels. *Journal of Hydraulic Engineering* 114, 738–756.
- 350 Chiu, C.L., 1991. Application of entropy concept in open-channel flow study. *Journal of Hydraulic Engineering* 117,  
351 615–628.
- 352 Chiu, C.L., Hsu, S.M., 2006. Probabilistic approach to modeling of velocity distributions in fluid flows. *Journal of*  
353 *Hydrology* 316, 28–42.
- 354 Chiu, C.L., Said, C., 1995. Maximum and mean velocities and entropy in open-channel flow. *Journal of Hydraulic*  
355 *Engineering* 121, 26–35.
- 356 Creutin, J., Muste, M., Bradley, A., Kim, S., Kruger, A., 2003. River gauging using piv techniques: a proof of concept  
357 experiment on the Iowa River. *Journal of Hydrology* 277, 182–194.
- 358 De Prony, G., 1804. *Recherches physico-mathématiques sur la théorie du mouvement des eaux courantes*. Imprimerie  
359 Impériale, Paris.
- 360 Dulos, P., 1877. *Cours de mécanique à l'usage des Ecoles d'Arts et Métiers et de l'enseignement spécial des Lycées*.  
361 Gauthier-Villard.
- 362 Fujita, I., 1997. Surface velocity measurement of river flow using video images of an oblique angle, in: *Proceedings of*  
363 *the 27th Congress of IAHR, San Francisco, CA*, pp. 227–232.
- 364 Fujita, I., Komura, S., 1994. Application of video image analysis for measurements of river surface flows. *Proceedings*  
365 *of Hydraulic Engineering* 38, 733–738.
- 366 Fujita, I., Notoya, Y., Tani, K., Tateguchi, S., 2019. Efficient and accurate estimation of water surface velocity in STIV.  
367 *Environmental Fluid Mechanics* 19, 1363–1378. doi:10.1007/s10652-018-9651-3.
- 368 Fujita, I., Watanabe, H., Tsubaki, R., 2007. Development of a non-intrusive and efficient flow monitoring technique: The  
369 space-time image velocimetry (stiv). *International Journal of River Basin Management* 5, 105–114.
- 370 Fulford, J., Sauer, V., 1986. Comparison of velocity interpolation methods for computing open-channel discharge. *Water*  
371 *Supply Paper* 2290. US Geological Survey. doi:10.3133/wsp2290.
- 372 Fulton, J., Ostrowski, J., 2008. Measuring real-time streamflow using emerging technologies: Radar, hydroacoustics,  
373 and the probability concept. *Journal of Hydrology* 357, 1–10.
- 374 Gunawan, B., Sun, X., Sterling, M., Shiono, K., Tsubaki, R., Rameshwaran, P., Knight, D., Chandler, J., Tang, X., Fujita,  
375 I., 2012. The application of LS-PIV to a small irregular river for inbank and overbank flows. *Flow Measurement and*  
376 *Instrumentation* 24, 1–12.
- 377 Jaynes, E., 1957. Information theory and statistical mechanics. *Physical Review* 106, 620–630.
- 378 Jaynes, E., 2003. *Probability theory: The logic of science*. Cambridge university press.
- 379 Kästner, K., Hoitink, A., Torfs, P., Vermeulen, B., Ningsih, N.S., Pramulya, M., 2018. Prerequisites for accurate moni-  
380 toring of river discharge based on fixed-location velocity measurements. *Water Resources Research* 54, 1058–1076.
- 381 Kumbhakar, M., Ghoshal, K., Singh, V., 2019. Two-dimensional distribution of streamwise velocity in open channel  
382 flow using maximum entropy principle: Incorporation of additional constraints based on conservation laws. *Computer*  
383 *Methods in Applied Mechanics and Engineering* 361, 112738.
- 384 Le Coz, J., Camenen, B., Peyrard, X., Dramais, G., 2012. Uncertainty in open-channel discharges measured with the  
385 velocity-area method. *Flow Measurement and Instrumentation* 26, 18–29.
- 386 Le Coz, J., Hauet, A., Pierrefeu, G., Dramais, G., Camenen, B., 2010. Performance of image-based velocimetry (Ispiv)  
387 applied to flash-flood discharge measurements in mediterranean rivers. *Journal of hydrology* 394, 42–52.
- 388 Luo, H., Singh, V., Schmidt, A., 2018. Comparative study of 1D entropy-based and conventional deterministic velocity  
389 distribution equations for open channel flows. *Journal of Hydrology* 563, 679–693.
- 390 Manfreda, S., Pizarro, A., Moramarco, T., Cimorelli, L., Pianese, D., Barbeta, S., 2020. Potential advantages of flow-  
391 area rating curves compared to classic stage-discharge-relations. *Journal of Hydrology* 585, 124752.
- 392 Marini, G., Fontana, N., 2020. Mean velocity and entropy in wide channel flows. *Journal of Hydrologic Engineering* 25,  
393 06019009.
- 394 Marini, G., Fontana, N., Singh, V., 2017. Derivation of 2d velocity distribution in watercourses using entropy. *Journal*  
395 *of Hydrologic Engineering* 22, 04017003.
- 396 Moramarco, T., Barbeta, S., Bjerklie, D., Fulton, J., Tarpanelli, A., 2019. River bathymetry estimate and discharge  
397 assessment from remote sensing. *Water Resources Research* 55, 6692–6711.
- 398 Moramarco, T., Barbeta, S., Tarpanelli, A., 2017. From surface flow velocity measurements to discharge assessment by  
399 the entropy theory. *Water* 9, 120.
- 400 Moramarco, T., Saltalippi, C., Singh, V., 2004. Estimation of mean velocity in natural channels based on chiu's velocity  
401 distribution equation. *Journal of Hydrologic Engineering* 9, 42–50.
- 402 Moramarco, T., Singh, V., 2010. Formulation of the entropy parameter based on hydraulic and geometric characteristics  
403 of river cross sections. *Journal of Hydrologic Engineering* 15, 852–858.
- 404 Mueller, D., 2013. *extrap*: Software to assist the selection of extrapolation methods for moving-boat adcp streamflow

405 measurements. *Computers & Geosciences* 54, 211–218.  
406 Muste, M., Fujita, I., Hauet, A., 2008. Large-scale particle image velocimetry for measurements in riverine environments.  
407 *Water Resources Research* 40.  
408 Nezu, I., Nakagawa, H., 1993. *Turbulence in open-channel flows*, iahr monograph series. A.A. Balkema, Rotterdam ,  
409 1–281.  
410 Perks, M., 2020. Klt-iv v1. 0: image velocimetry software for use with fixed and mobile platforms. *Geoscientific Model*  
411 *Development* 13, 6111–6130.  
412 Rantz, S., 1982. Measurement and computation of streamflow. *Water Supply Paper 2175*. US Geological Survey.  
413 doi:10.3133/wsp2175.  
414 Shannon, C., 1948. A mathematical theory of communication. *The Bell System Technical Journal* 27, 623–656.  
415 Singh, V.P., 2014. *Entropy Theory in Hydraulic Engineering: An Introduction*. American Society of Civil Engineers.  
416 Tauro, F., Piscopia, R., Grimaldi, S., 2019. PTV-Stream: A simplified particle tracking velocimetry framework for  
417 stream surface flow monitoring. *CATENA* 172, 378–386.  
418 Yeganeh, M., Heidari, M., 2020. Estimation of one-dimensional velocity distribution by measuring velocity at two points.  
419 *Flow Measurement and Instrumentation* 73, 101737.